DOI: 10.61782/fa.2025.0499

FORUM ACUSTICUM
EURONOISE 2025

INVESTIGATING THE EFFECT OF SKIN AND HAIR ABSORPTION ON NUMERICALLY SIMULATED HRTFS

Fabian Brinkmann* **Tim Niklas Wennemann** **Stefan Weinzierl**

Audio Communication Group, Technische Universität Berlin, Germany

ABSTRACT

Head-Related Transfer Functions (HRTFs) are a fundamental building block of headphone-based 3D audio, and the use of individual HRTFs will improve audio quality in many cases. As an alternative to time-consuming acoustic measurements, individual HRTFs can be numerically simulated based on 3D head meshes using the Boundary Element Method. Although previous studies have shown that impedance effects have an influence on the HRTF, the sound absorption of skin and hair is usually neglected in numerical simulations. To improve these, we developed a simplified hair absorption model based on available measurements of hair impedance and used it with an existing skin impedance model to simulate HRTFs for 54 different head meshes. The effect of non-rigid boundary conditions introduces small but audible spectral differences. Considering skin impedance alone already reduces unnatural resonance peaks that are often observed in HRTFs simulated with rigid boundary conditions but not in acoustically measured HRTFs. The additional integration of hair absorption further reduces these resonances and adds high-frequency attenuation above about 1 kHz, which can reach attenuations of 10 dB and more depending on the source position and the amount of hair absorption.

Keywords: *head-related transfer function, boundary condition, skin, hair*

**Corresponding author*: *fabian.brinkmann@tu-berlin.de.*

1. INTRODUCTION

Head-related transfer functions (HRTFs) describe the directional filtering of incoming sound due to scattering, diffraction, and reflection at the human ears, head, and torso. They contain individual spectral and interaural cues that are interpreted by the auditory system to derive an internal representation of the acoustic scene surrounding the listener. Thus, HRTFs are the basis for headphone-based 3D audio rendering. Moreover, percepts such as the perceived sound color and spatial location of a sound source are directly related to the HRTF [1]. Acoustic measurements are often considered to be the most valid way to obtain HRTFs, but such measurements require a specially equipped laboratory and are time consuming for the subjects who have to visit the laboratory. For these reasons, measurements are not suitable for generating large HRTF databases such as those required for learning-based HRTF individualization [2].

Numerical simulations [3, 4] can be an alternative solution to obtain an arbitrary number of HRTF sets from head and ear shapes generated by 3D morphable models, also termed parametric models [5, 6]. While numerically simulated HRTFs can be close to measured HRTFs for dummy heads [7, 8], differences between simulated and measured human HRTFs are larger resulting for example in localization and coloration errors [9]. The reasons for the increased differences are not entirely clear, but it seems reasonable that the current best practice of simulating HRTFs from head-only meshes and ignoring skin, hair, and cloth absorption when simulating rigid boundary conditions are contributing factors.

Relatively few studies have investigated the effect of non-rigid boundary conditions on simulated HRTFs. Katz [10] simulated HRTFs up to 5.5 kHz for a single hair impedance according to frontal incidence impedance

measurements [11]. The results showed relatively small effects for most source positions and attenuation of up to 6 dB for contralateral sources and sources from above. Ghorbal et al. [12] optimized the impedance to minimize the mean squared magnitude error between measured and simulated HRTFs. They found that considering impedance reduces the average error across source positions by up to 58% (7.5 dB) between 6.5 and 13 kHz. Localization experiments additionally found that polar errors (angular errors in vertical direction) are comparable to those observed with measured HRTFs when considering impedance, while quadrant errors (a measure for font/back and up/down confusion) are still slightly larger. Treeby et al. [13, 14] analytically evaluated the effect of hair using a spherical head model divided into two hemispheres, one with rigid boundary conditions and the other with a hair impedance. They found potentially audible effects on interaural level differences and probably inaudible effects on interaural time differences. However, these studies used only a spherical head [13] or single head mesh with either realistic impedance conditions but simulations with a limited frequency range [10] or unrealistic impedance conditions but full-range simulations [12]. While Katz [10] considered skin to be acoustically rigid, Hajarolasvadi et al. [15] and Di Giusto et al. [16] showed that considering skin impedance and skin like material impedance can reduce the difference to measured data. Specifically, including skin impedance decreased the magnitude of a resonances [15].

In the current study, we investigate the influence of realistic skin and hair absorption on simulated HRTFs using head meshes from the HUTUBS database [9]. Section 2 introduces the skin and hair absorption model, the automatic segmentation of head meshes into skin and hair regions, and the numerical HRTF simulation. Section 3 details the results, and concluding remarks, along with indications of limitations of the current study and possible future work, are given in section 4.

2. METHOD

The following describes the HRTF simulations including the impedance boundary conditions used, the automatic segmentation of the head meshes into skin and hair regions, and the numerical simulations.

2.1 Boundary Conditions

We used the skin impedance model of Håkansson et al. [17], which is a three-parameter model derived from mechanical impedance measurements

$$Z_s = \frac{R_s}{A_t} + \frac{\mathrm{j}\omega L_s}{A_t} + \frac{1}{\mathrm{j}\omega C_s A_t} \tag{1}$$

with the damping (resistive impedance) $R_s = 9\,\mathrm{Nsm}^{-1}$, mass (inductive impedance) $L_s = 0.53 \cdot 10^{-3}\,\mathrm{Ns}^2/\mathrm{m}$, compliance (capacitive impedance) $R_s = 5.3 \cdot 10^{-6}\,\mathrm{m/N}$, the exitation area $A_t = 1.5\,\mathrm{cm}^2$, and the imaginary unit j.

No such model exists for the impedance of hair, and existing measurements by Katz [11] and Treeby et al. [18], who measured the normal impedance of five and eight human hair samples, respectively, have a limited frequency range of 400 Hz to 6 kHz. We digitized the existing data using WebPlotDigitizer [19], and to facilitate the extrapolation, we decided to assume purely resistive impedances by converting all data to real-valued absorption coefficients [20]

$$\alpha = \frac{4\Re(Z)}{(\Re(Z)+1)^2 + \Im(Z)^2} \tag{2}$$

with $\Re(\cdot)$ and $\Im(\cdot)$ denoting the real and imaginary part. In the next step, we approximated the measured hair absorption data as a simple linear function of frequency

$$\alpha_l(f) = \frac{m}{10^5} f \tag{3}$$

with the slope parameter m. In a final step, the hair absorption was clipped by the skin absorption α_s and a maximum value of one

$$\alpha_h = \begin{cases} \alpha_s & \text{if } \alpha_l \leq \alpha_s \\ \alpha_l & \text{if } \alpha_s < \alpha_l < 1 \\ 1 & \text{if } \alpha_s \geq 1 \end{cases} \tag{4}$$

to yield the final hair absorption model.

Figure 1 shows all measured and modeled absorption curves. We chose to use the skin boundary condition and nine additional hair boundary conditions. We chose slope coefficients m according to (3) to roughly span the range between skin absorption and measured absorption values from the literature. For numerical simulations, the absorption values were converted to specific admittances

$$Y_{\text{specific}} = \frac{1-\sqrt{1-\alpha}}{1+\sqrt{1-\alpha}}, \tag{5}$$

which increases the flexibility of the simulations since Y_{specific} is independent of the speed of sound and air density. Note that the impedance curves were included in

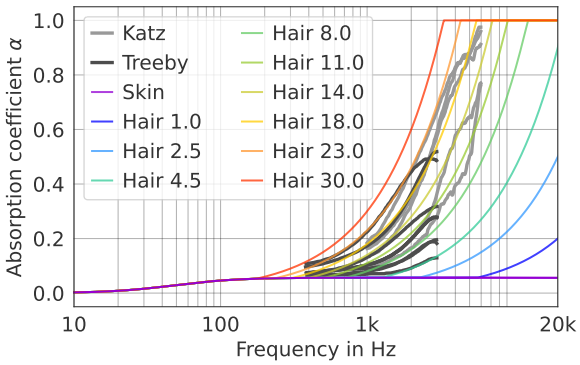

Figure 1. Measured and modeled absorption coefficients. Numbers give slope m according to (3).

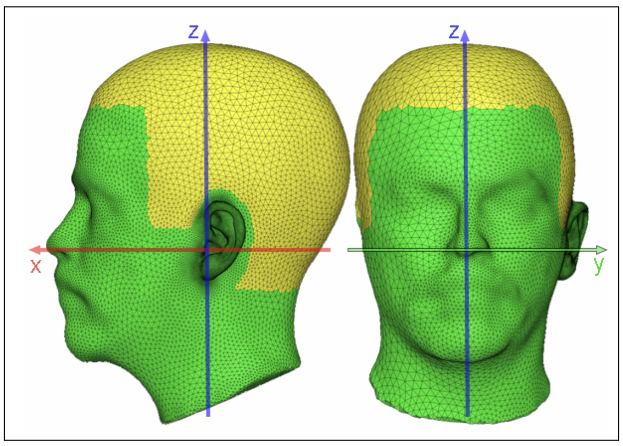

Figure 2. Example for a mesh after segmentation into skin (green) and hair (yellow) regions.

the numerical simulation in the direction of the surface normal. The consequences of this simplification are discussed in Section 4.

2.2 Mesh Segmentation

Each element of a head mesh must be assigned to a boundary condition—rigid, skin, or hair in this case—which requires a segmentation of the mesh. To be generalizable, we used an automatic segmentation based on anthropometric features similar to Katz [10]. Figure 2 shows an example of a head mesh after segmentation.

The hair region was assigned in several heuristically derived steps: First, all mesh elements at the top of the head within the range $z \geq 0.7 z_{\text{max}}$ were classified as hair, where z_{max} is the z coordinate of the top vertex. Second, the elements at the back of the head within the ranges $x \leq 0.2 x_{\text{min}}$ and $z \geq -0.2 z_{\text{max}}$ were selected, where x_{min} is the value of the element with the smallest x-coordinate. Third, mesh elements that satisfy the conditions $x \leq 0.5 x_{\text{max,hair}}$ and $z \geq 0.1 z_{\text{max}}$ are also defined as hair, where $x_{\text{max,hair}}$ is the value of the previously selected hair element with the largest x-coordinate. The above erroneously assigned some elements on the ear to skin, which was corrected in the next step where all elements within an ellipse centered at the ear canal entrance were assigned to skin. The size and rotation of the ellipse were determined using the anthropometric ear measurements d_i provided as part of the HUTUBS HRTF database. The major axis of the ellipse was defined as twice the sum of the cavum concha height, the cymba concha height, and the fossa height $2(d_1 + d_2 + d_4)$. The minor axis was taken as 2.5 times the pinna width d_6. Additionally, the ellipse was rotated by the pinna rotation angle Θ_1 (see [9] for a detailed definition of the anthropometric parameters). Since the ellipse deselected elements in front of the ear that should be part of the hair mask, these elements were reassigned in a final step. Elements between $0 \leq x \leq x_{\text{max,hair}}$ and $z \geq 0.1 z_{\text{max}}$ were assigned to the hair mask if they were in front of the plane through the points $\mathbf{p}_1 = \{x = 0.015; z = 0.1 z_{\text{max}}\}$ m and $\mathbf{p}_2 = \{x = 0; z = 0.3 z_{\text{max}}\}$ m.

Note that we used a modified version of the HUTUBS head meshes, with the meshes slightly translated and rotated to better match the microphone position and head orientation to the pictures of the subjects taken during the acoustic measurements.

2.3 Numerical HRTF Simulations

We simulated HRTFs using Mesh2HRTF similar to the workflow described by Brinkmann et al. [3]: Separate simulations were performed for the left and right ear. To speed-up simulations, acoustic reciprocity was exploited by switching the position of sources and receivers. To this end, we used a volume velocity source by assigning a velocity boundary condition to the mesh element at the center of the blocked ear canal entrance and placed ideal receivers at the position of the 440 loudspeakers used in the HUTUBS database. For further speed-up, we used the multi-level fast multipole boundary element method (ML-FMM-BEM, cf. [4]) and graded the meshes. Mesh grading reduces the number of elements in the mesh by increasing their size with increasing distance from the vol-

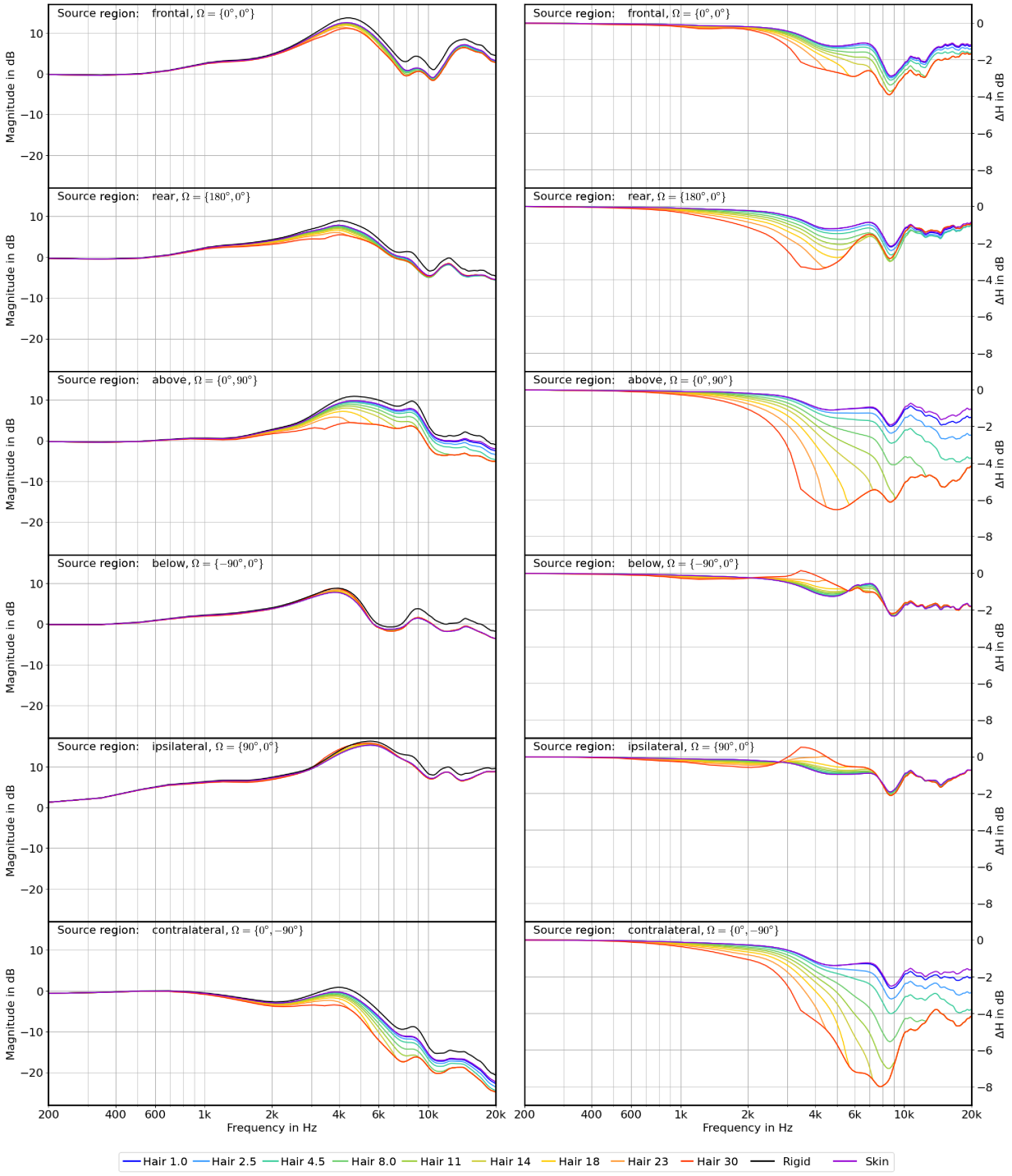

Figure 3. Effect of simulated skin and hair absorption averaged across subjects and ears for six different source regions. The left column shows averaged HRTFs and the right column the difference ΔH. Numbers give slope m according to (3).

ume velocity source [21]. Assuming a temperature of 20°C and a relative humidity of 50%, we set the speed of sound to 343.2 $\mathrm{m/s}$ and the density of air to 1.2 $\mathrm{kg/m^3}$.

For each of the 54 head meshes, we simulated HRTFs for each ear and 11 boundary conditions (rigid, skin, and 9 hair materials, cf. Fig. 1). HRTFs were computed for 129 equidistant frequencies between 0 Hz and 22.05 kHz.

3. RESULTS

The following sections detail the results, with a focus on examining general effects by averaging HRTFs across subjects and/or source positions. We use spherical coordinates with the azimuth angle $-180° \leq \varphi \leq 180°$ (0°: front, 90°: left, −90°: right, ±180°: back) and elevation angle $-90° \leq \vartheta < 90°$ (90°: above, 0°: front, −90°: below). We jointly analyze left and right ears by changing the sign of the azimuth angle for right ear HRTFs.

3.1 Effect of source position

Figure 3 shows the effect of skin and hair absorption for six source regions averaged across subjects and ears. A source region is defined by an anchor position $\Omega = \{\varphi, \vartheta\}$ and contains all sources within a great circle distance of 25° from the anchor. To help interpreting the data, we also show the difference between simulations with rigid and non-rigid boundary conditions $\Delta H = |H_{\text{rigid}}|/|H_{\text{non-rigid}}|$ where H denotes the complex HRTF spectrum. In general, increased absorption results in less energy in the HRTFs, or in other words an increased damping with respect to the rigid boundary condition. The damping exceeds 1 dB above 2 kHz and the maximum damping occurs between 5 kHz and 9 kHz depending on the source region. The effect of skin absorption is rather independent of the source region and causes damping between 1 dB and 2 dB above 4 kHz. Apart from this, the source region clearly affects the amount of damping.

The damping is highest for contralateral sources and sources from above, where the sound is diffracted around large parts of the hair region before reaching the ear. In these cases, damping between 6 dB and 8 dB is visible for $m \gtrapprox 14$. For sources from above the largest damping is already reached at 4 kHz, where the human auditory system is most sensitive. Intermediate damping between 3 dB and 4 dB for $m \gtrapprox 8$ can be observed for frontal and rear source regions due to sound diffraction around at least small hair regions, and the smallest effects are visible for sources from below—where the sound diffracts only around skin

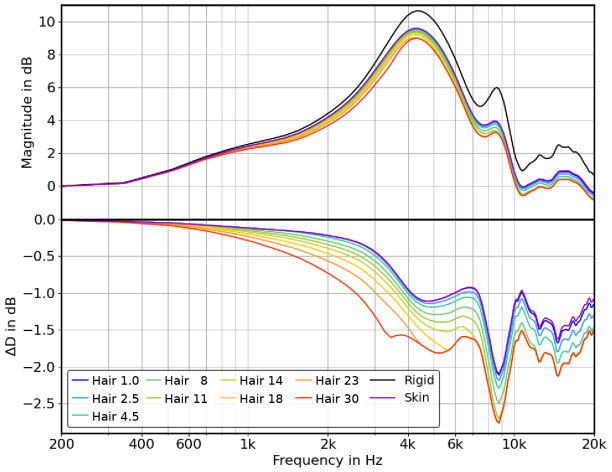

Figure 4. Diffuse field transfer functions (top) and effect of skin and hair absorption (bottom). Numbers give slope m according to (3).

regions before reaching the ear—and ipsilateral sources—where the sound reaches the ear directly. For these source regions, the maximum damping is about 2 dB. Somewhat counterintuitively, a slight boost in energy of less than 1 dB between 3 kHz and 4 kHz can be observed for the most absorbing hair with $m = 30$. This might be explained by multi-path sound propagation: Since sound can fully diffract around the head, the diffracted sound can reach the ear with an additional delay according to the diffraction path length. If the diffracted sound arrives with a phase shift of $\approx 180°$, it causes a deconstructive superposition and thus a loss in energy. This energy loss is avoided, if the diffracted sound is absorbed before reaching the ear, which would result in an energy boost compared to less absorbing boundary conditions where the diffracted sound energy is not completely absorbed.

An analysis of the damping across all source positions—not shown here due to page limitations—showed that damping is largest for sources around $\Omega = \{-60°, -60°\}$ when considering only skin absorption ($\Delta H \approx 1.5$ dB averaged across subjects and frequency) and for sources around $\Omega = \{-110°, 50°\}$ when additionally considering hair absorption ($\Delta H \approx 10$ dB for $m = 30$). To assess the overall effect, we computed the diffuse field transfer function by averaging across all source positions (cf. Fig. 4). This shows that skin absorption causes a damping of approximately 1 dB above 4 kHz, while adding more absorptive hair material increases this

effect only slightly to about 1.5 dB to 2 dB.

3.2 Effect of head mesh

So far, we investigated the effect of skin and hair absorption averaged across subjects, but it is worth noting that there is considerable variance between subjects. Figure 5 illustrates this for the contralateral source region and subjects pp2 and pp10 from the HUTUBS database. Two observations can be made: First, the effect of absorption is generally smaller for subject pp2 with a maximum damping of about 5 dB compared to subject pp10 with a maximum damping of about 12.5 dB. Second, the HRTFs simulated with the rigid boundary condition show strong peaks for pp10 that are almost invisible for pp2. The peaks of pp10 are most prominent at high frequencies, appearing at approximately 8, 11, 14, 17, and 20 kHz. Spectral peaks in HRTFs are most likely caused by resonances inside the pinna cavities [22], but we are not aware of any example of a measured HRTF where these peaks are so prominent. Hence, it seems likely that their prominence is caused by assuming perfectly rigid boundary conditions. This assumption is supported by the fact that damping is largest at or close to the center frequencies of spectral peaks, and the strength of the resonance peaks is already clearly reduced if applying only skin absorption. Between the peaks, the damping is roughly comparable for pp2 and pp10. In addition, but less clearly, the concha resonance at about 4 kHz is also more pronounced for pp10. While the difference is only 1 dB in this case, it could introduce coloration in the frequency range where the human auditory system is most sensitive.

We observed similar effects for other subjects, with an effect strength somewhere between subject pp2—showing the smallest overall damping of all subjects—and pp10—showing the largest overall damping. Moreover, the resonances and variance between subjects are more pronounced for source regions where damping is large (see previous section). Potentially, this is the case because resonances can be excited with low energy and are more clearly visible when the spectrum contains less energy to the left and right of the resonance center frequencies.

4. CONCLUSION AND FUTURE WORK

We have investigated the effect of skin and hair absorption on numerically simulated HRTFs. To the best of our knowledge, this is the first time that this has been done for multiple head meshes and absorption curves that systematically cover the range between skin absorption and the maximum absorption that can be expected from hair. In agreement with Katz [10] and Treeby et al. [18], we observed that hair-induced damping increases with the path length that the sound has to travel through/along the hair. Thus, the largest effects occur for contralateral and elevated source regions. While Katz [10] reported a maximum damping of 6 dB for frequencies below 5.5 kHz, we observed a maximum of 12.5 dB at about 7 kHz. Clearly, these differences are due to the limited frequency range and number of subjects in the Katz study.

In contrast to Katz [10] and Blauert [1], who stated that skin can be assumed to be acoustically rigid, we observed a strong reduction of the HRTF resonance peaks when only skin absorption is applied. This is in line with simulations by Hajarolasvadi et al. [15] and Di Giusto et al. [16]. Since the observed resonance peaks in simulated HRTFs with rigid boundary conditions do not appear in measured HRTFs, we conclude that assuming skin to be acoustically rigid is not correct. Although informal listening has shown that the perceptual effect of skin absorption in HRTFs is small, we recommend using skin absorption instead of a rigid boundary condition as a new default for simulating HRTFs.

It can be hypothesized that the perceptual effect of hair is also small on average (cf. Fig. 4). However, it is also reasonable to assume that there are specific source positions and use cases where it will be relevant. While Treeby et al. [13, 14] have already shown the influence of hair on interaural level differences, more detailed investigations including perceptual experiments and or auditory modeling are needed, for example regarding median plane localization or coloration.

We have assumed real-valued, purely resistive impedance conditions for simplicity. It should be noted that Treeby et al. [14] showed that the phase of the impedance can affect the ILD of a modified spherical head by up to 5 dB. While this change can be assumed to be audible, accurately considering the phase of hair impedance may be impractical because this property may be specifically hard to estimate for actual humans. With this in mind it should be mentioned, that estimating acoustic hair properties in a more practical way, for example from images of a subject, is currently an unsolved problem beyond the scope of this article. Furthermore, and as already mentioned by Katz [10], the BEM considers only locally reacting impedance conditions normal to the mesh surface, which is a rough approximation neglecting gazing incidence and the fact that hair is a voluminous material through which sound travels in reality. Treeby et al [13]

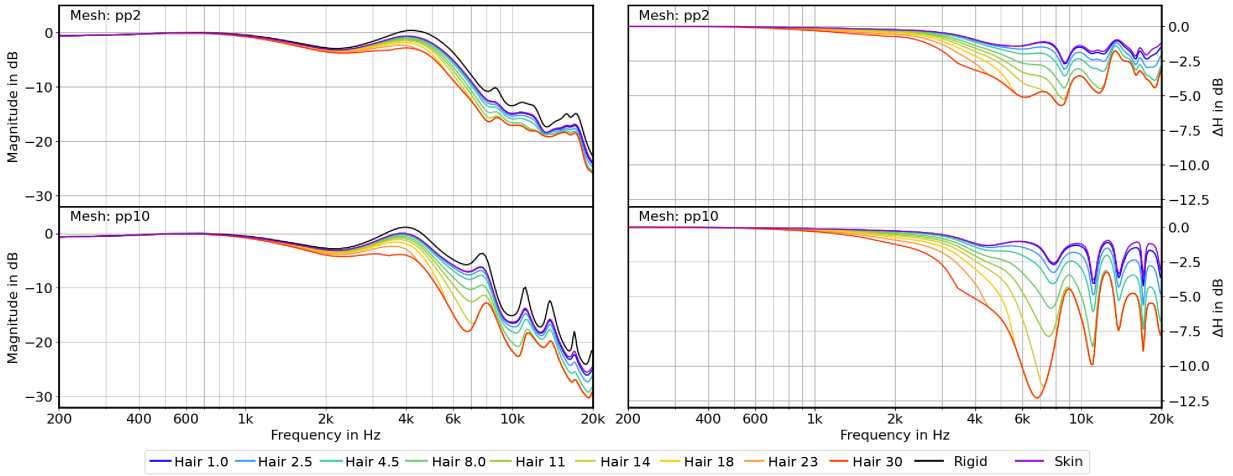

Figure 5. HRTFs and ΔH for the contralateral source region and subjects pp2 and pp10. Numbers give slope m according to (3).

applied locally reacting normal impedance conditions to a spherical head model and found good agreement with data. Thus, it may be possible to achieve realistic results with this simplified impedance model, but this should be further verified against measured data and/or FEM simulations where voluminous material can be modeled.

We observed high inter-subject variance and hypothesized that this is mostly caused by differently pronounced resonance peaks in HRTFs simulated with rigid boundary conditions. This is supported by further investigations—not shown here due to page limitations—where we tried to correlate the damping with anthropometric features such as the head width, depth, and height, as well as with the hair area of each mesh without success. To rule this out more clearly, the computation of $DeltaH$ could be adapted to show the damping with respect to HRTFs simulated with skin absorption $\Delta H_{\text{hair}} = |H_{\text{skin}}|/|H_{\text{hair}}|$. If our assumption is correct, this should reduce the inter-subject variance and allow for a more systematic investigation of the remaining between-subject effects. In addition, it would be interesting to examine why resonance peaks in HRTFs are so differently pronounced in simulated HRTFs.

Lastly, we restricted the current analysis to HRTFs averaged across sources, subjects, and ears as a first attempt to generalize the effect of skin and hair absorption. Future work could also explore this in more detail without applying any averaging before the analysis.

5. REFERENCES

[1] J. Blauert, *Spatial Hearing. The Psychophysics of Human Sound Localization*. Cambridge, Massachusetts: MIT Press, revised ed., 1997.

[2] D. Fantini, M. Geronazzo, F. Avanzini, and S. Ntalampiras, "A Survey on Machine Learning Techniques for Head-Related Transfer Function Individualization," *IEEE Open Journal of Signal Processing*, Jan. 2025.

[3] F. Brinkmann, W. Kreuzer, J. Thomsen, S. Dombrovskis, K. Pollack, S. Weinzierl, and P. Majdak, "Recent Advances in an Open Software for Numerical HRTF Calculation," *J. Audio Eng. Soc.*, vol. 71, pp. 502–514, July 2023.

[4] W. Kreuzer, K. Pollack, F. Brinkmann, and P. Majdak, "NumCalc: An open-source BEM code for solving acoustic scattering problems," *Engineering Analysis with Boundary Elements*, vol. 161, pp. 157–178, Apr. 2024.

[5] F. Pausch, F. Perfler, N. Holighais, and P. Majdak, "Comparison of Deep-Neural-Network Architectures for the Prediction of Head-Related Transfer Functions Using a Parametric Pinna Model," in *Forum Acusticum*, (Torino, Italy), Sept. 2023.

[6] S. Jain, F. Brinkmann, J. Fan, M. Kohlbrenner, R. Moeller, and S. Weinzierl, "A 3D morphable head and a pinna model for HRTF Individualization,"

in *DAS|DAGA - 51st Annual Meeting on Acoustics*, (Copenhagen, Denmark), Mar. 2025.

[7] F. Brinkmann, A. Lindau, S. Weinzierl, S. van de Par, M. Müller-Trapet, R. Opdam, and M. Vorländer, "A High Resolution and Full-Spherical Head-Related Transfer Function Database for Different Head-Above-Torso Orientations," *J. Audio Eng. Soc.*, vol. 65, pp. 841–848, Oct. 2017.

[8] S. T. Prepeliță, J. Gómez Bolaños, M. Geronazzo, R. Mehra, and L. Savioja, "Pinna-related transfer functions and lossless wave equation using finite-difference methods: Validation with measurements," *J. Acoust. Soc. Am.*, vol. 147, pp. 3631–3645, May 2020.

[9] F. Brinkmann, M. Dinakaran, R. Pelzer, P. Grosche, D. Voss, and S. Weinzierl, "A cross-evaluated database of measured and simulated HRTFs including 3D head meshes, anthropometric features, and headphone impulse responses," *J. Audio Eng. Soc.*, vol. 67, pp. 705–718, Sept. 2019.

[10] B. F. G. Katz, "Boundary element method calculation of individual head-related transfer function. II. Impedance effects and comparisons to real measurements," *J. Acoust. Soc. Am.*, vol. 110, pp. 2449–2455, Nov. 2001.

[11] B. F. G. Katz, "Acoustic absorption measurement of human hair and skin within the audible frequency range," *J. Acoust. Soc. Am.*, vol. 108, pp. 2238–2242, Nov. 2000.

[12] S. Ghorbal, X. Bonjour, and R. Séguier, "On the importance of impedance for perceptual relevance of HRTF," in *148th AES Convention*, (Vienna, Austria), p. Paper 10354, May 2020.

[13] B. E. Treeby, J. Pan, and R. M. Paurobally, "The effect of hair on auditory localization cues," *J. Acoust. Soc. Am.*, vol. 122, pp. 3586–3597, Dec. 2007.

[14] B. E. Treeby, R. M. Paurobally, and J. Pan, "The effect of impedance on interaural azimuth cues derived from a spherical head model," *J. Acoust. Soc. Am.*, vol. 121, pp. 2217–2226, Apr. 2007.

[15] S. Hajarolasvadi, B. Essink, P. F. Hoffmann, A. Ng, U. Skov, and S. T. Prepeliţă, "Digital Twin of a Head and Torso Simulator: Validation of Far-Field Head-Related Transfer Functions with Measurements," in *AES Int. Conf. Audio for Virtual and Augmented Reality (AVAR)*, (Redmond, WA, USA), Aug. 2022.

[16] F. Di Giusto, Sinev, K. Pollack, S. van Ophem, and E. Deckers, "Analysis of impedance effects on head-related transfer functions of 3D printed pinna and ear canal replicas," in *Forum Acusticum*, (Torino, Italy), Sept. 2023.

[17] B. Håkansson, P. Carlsson, and A. Tjellström, "The mechanical point impedance of the human head, with and without skin penetration," *J. Acoust. Soc. Am.*, vol. 80, pp. 1065–1075, Oct. 1986.

[18] B. E. Treeby, J. Pan, and R. M. Paurobally, "An experimental study of the acoustic impedance characteristics of human hair," *J. Acoust. Soc. Am.*, vol. 122, pp. 2107–2117, Oct. 2007.

[19] A. Rohatgi, "WebPlotDigitizer v5.2." `https://automeris.io`, Aug. 2024. (accessed 2025-04-03).

[20] M. Möser, *Engineering Acoustics: An Introduction to Noise Control*. Berlin Heidelberg: Springer, 2 ed., 2009.

[21] T. Palm, S. Koch, F. Brinkmann, and M. Alexa, "Curvature-adaptive mesh grading for numerical approximation of head-related transfer functions," in *Fortschritte Der Akustik – DAGA 2021*, (Vienna, Austria), pp. 1111–1114, Aug. 2021.

[22] H. Takemoto, P. Mokhtari, H. Kato, R. Nishimura, and K. Iida, "Mechanism for generating peaks and notches of head-related transfer functions in the median plane," *J. Acoust. Soc. Am.*, vol. 132, pp. 3832–3841, Dec. 2012.